Journal of Asian Ceramic Societies 3 (2015) 64–69

View metadata, citation and similar papers at core.ac.uk

brought to you by CORE

provided by Elsevier - Publisher Connector

Journal of Asian Ceramic Societies

journal homepage: www.elsevier.com/locate/jascer

Optical properties of nanocrystalline HfO_2 synthesized by an auto-igniting combustion synthesis

H. Padma Kumar[a,*], S. Vidya[b], S. Saravana Kumar[c], C. Vijayakumar[d], Sam Solomon[b], J.K. Thomas[b]

[a] Department of Physics, V.T.M.N.S.S. College, Dhanuvachapuram, Kerala 695503, India
[b] Electronic Materials Research Laboratory, Department of Physics, Mar Ivanios College, Thiruvananthapuram, Kerala 695015, India
[c] Department of Physics, N.S.S. College, Pandalam, Kerala 689501, India
[d] Department of Physics, St. Jude's College, Thoothoor, Tamil Nadu 629176, India

ARTICLE INFO

Article history:
Received 26 August 2014
Received in revised form 22 October 2014
Accepted 26 October 2014
Available online 15 November 2014

Keywords:
Nanomaterials
Materials processing
Combustion synthesis
Ceramics
Photoluminescence
Optical properties

ABSTRACT

The optical properties of nanocrystalline HfO_2 synthesized using a single-step auto-igniting combustion technique is reported. Nanocrystalline hafnium oxide having particle size of the order 10–15 nm were obtained in the present method. The nanopowder was characterized using X-ray diffraction, Fourier transform infrared and Fourier transform Raman spectroscopic studies. All these studies confirm that the phase formation is complete in the combustion synthesis and monoclinic phase [$P2_1/c(14)$] of HfO_2 is obtained without the presence of any impurities or additional phases. The powder morphology of the as-prepared sample was studied using transmission electron microscopy and the results were in good agreement with that of the X-ray diffraction studies. The optical constants such as refractive index, extinction coefficient, optical conductivity and the band gap were estimated from UV–vis spectroscopic techniques. The band gap of nanocrystalline HfO_2 was found to be 5.1 eV and the sample shows a broad PL emission at 628 nm. It is concluded that the transitions between intermediate energy levels in the band gap are responsible for the interesting photoluminescent properties of nanocrystalline HfO_2.

© 2014 The Ceramic Society of Japan and the Korean Ceramic Society. Production and hosting by Elsevier B.V. All rights reserved.

1. Introduction

Hafnium oxide (HfO_2) is an important ceramic material due to its high dielectric constant ($\varepsilon_r \sim 30$), high melting point (2758 °C) and greater chemical stability [1]. HfO_2 and its solid solutions with SiO_2 are promising replacements for SiO_2 for their potential applications as gate dielectrics [2]. Recently the optical applications of HfO_2 are gaining widespread interest. Due to its transparency over a wide range from ultraviolet to mid-infrared, it is used as materials for heat resistant, reflective and protective optical coating [3–5]. HfO_2 found promising optical coating applications such as filters, beam splitters, anti-reflection coating, high reflectivity mirrors, etc. [6,7].

Hafnium in bulk can adopt three different crystal structures at ambient temperatures. At room temperature it is stable in monoclinic structure, transforms to tetragonal at about 1720 °C and becomes cubic at about 2600 °C [8]. Synthesis of advanced ceramics and specialty materials as nanocrystals is one of the major challenges in the development of material processing technology [9]. The advantages of nanocrystalline materials are superior phase homogeneity, sinterability and microstructure leading to unique mechanical, electrical, dielectric, magnetic, optical and catalytic properties [10]. There have been increasing interests in the use of nanoparticles to optical systems because of their enhanced optical properties due to their smaller size [11]. Because of its high chemical stability, high cost and high processing temperatures, hafnium oxide is less studied in the form of nanomaterials than other simple oxides. Recently the synthesis of nanocrystalline hafnia by a sol–gel method was reported [12–14]. The synthesis of nanocrystalline HfO_2 by the hydrolysis of hafnium oxychloride in ethanol was reported [15]. The preparation of nanocrystalline HfO_2 by ultrasonically assisted hydrothermal treatment has also been reported [16].

Recently combustion synthesis technique has been reported as an easy, economical and time-saving method to synthesize advanced ceramic powders and functional materials [17–19]. Since solution mixing is generally used in combustion synthesis, it results in relatively ultra-phase homogeneity than in any other techniques. Generally in combustion synthesis, which uses PVA as a complexing agent and urea as fuel, it requires post-annealing or calcination of the precursor to get phase purity. Recently, with the use of citric

* Corresponding author. Tel.: +91 9495200830; fax: +91 471 2230919.
E-mail address: drhpadmakumar@gmail.com (H. Padma Kumar).
Peer review under responsibility of The Ceramic Society of Japan and the Korean Ceramic Society.

2187-0764 © 2014 The Ceramic Society of Japan and the Korean Ceramic Society. Production and hosting by Elsevier B.V. All rights reserved.
http://dx.doi.org/10.1016/j.jascer.2014.10.009

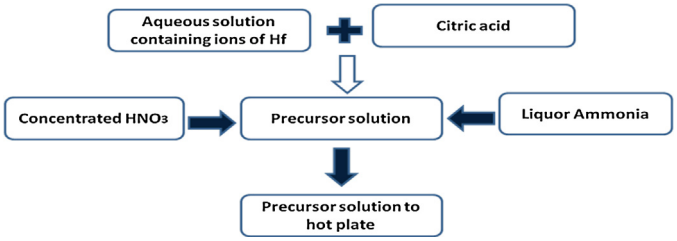

Fig. 1. Schematic diagram of the modified combustion synthesis technique.

acid as complexing agent and ammonia as fuel instead of PVA and urea, we were able to prepare a number of phase pure perovskites and scheelites as nanopowders in a single-step combustion itself, hence avoiding the need of post-annealing or calcination steps [18]. The powder thus obtained shows superior phase homogeneity, purity, improved sinterability, etc. than that of their conventional coarse-grained and micron-sized counterparts. However there are only a few reports available on the synthesis of nanocrystalline single oxides especially group IVB metals such as hafnia, zirconia, niobium, tin, etc., particularly hafnia, which are widely required as optical functional materials in opto-electronic devices. This may be due to the fact that pure hafnia is costly and availability is hard compared to the other group IVB metals. In the present paper, we focus our attention to prepare highly pure hafnia and report the single-step synthesis of hafnium oxide nanoparticles by a modified combustion synthesis technique, its structural characterization, particulate properties, photoluminescent and related properties. The process also explores a value addition in the synthesize of ultrafine nanocrystalline phase pure hafnium oxide from relatively low cost and easily available coarse-grained hafnium chloride powder.

2. Materials and methods

In the present study the modified auto-igniting combustion technique [20] was used for the synthesis of nanoparticles of HfO_2. In a typical synthesis, aqueous solution containing ions of Hf was prepared by dissolving high purity $HfCl_4$ (99%) in double distilled water (200 ml) in a glass beaker. Citric acid (99%) was then added to the solution containing Hf ions. Amount of citric acid was calculated based on total valence of the oxidizing and the reducing agents for maximum release of energy during combustion [20]. Oxidant/fuel ratio of the system was adjusted by adding nitric acid and ammonium hydroxide and the ratio was kept at unity. The solution containing the precursor mixture at a pH of ~7.0 was heated using a hot plate at ~250 °C in a ventilated fume hood. The solution boils on heating and undergoes dehydration accompanied by foam. The foam then gets ignited by itself and on persistent heating giving voluminous and fluffy product of combustion. The combustion product was subsequently characterized as single-phase nanocrystals of HfO_2. A schematic diagram of the modified combustion synthesis technique is shown in Fig. 1.

Structure of the as-prepared powder was examined by powder X-ray diffraction (XRD) technique using a X-ray Diffractometer (Model Bruker D-8) with nickel filtered CuK_α radiation. The structure was confirmed by using Raman spectroscopic studies. The Fourier transform-Raman spectrum of the nanocrystalline HfO_2 was carried out at room temperature in the wave number range 50–1200 cm^{-1} using Bruker RFS/100S Spectrometer at a power level of 150 mW and at a resolution of 4 cm^{-1}. The samples were excited with a Nd:YAG laser lasing at 1064 nm and the scattered radiations were detected using Ge detector. The infrared (IR) spectra of the samples were recorded in the range 400–4000 cm^{-1} on a Thermo-Nicolet Avatar 370 Fourier Transform Infrared (FTIR) Spectrometer using KBr pellet method. Particulate properties of the

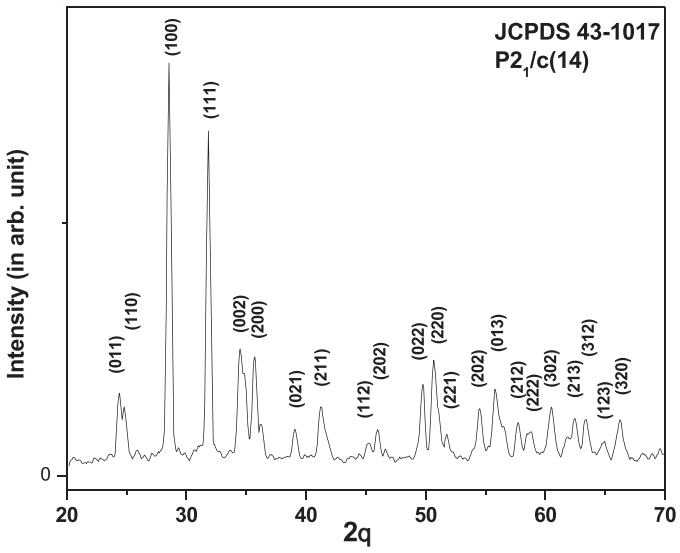

Fig. 2. XRD pattern of as-prepared HfO_2.

combustion product were examined using transmission electron microscopy (Model: JEOL JEM 1011) operating at 200 kV. The samples for transmission electron microscope (TEM) were prepared by ultrasonically dispersing the powder in methanol and allowing a drop of this to dry on a carbon-coated copper grid. The photoluminescence spectra of the samples were measured using Flurolog@-3 Spectroflurometer. The photons from the source were filtered by an excitation spectrometer. The monochromatic radiation was then allowed to fall on the disc samples and the resulting radiation was filtered by an emission spectrometer and then fed to a photomultiplier detector. The variation of intensity was recorded as a function of wavelength. The optical measurements of the nanopowders were carried out at room temperature using a Cary 100 BIO UV–vis spectrophotometer in the wavelength range from 190 to 900 nm by dispersing the nanopowder in ethanol taken in the 1:20 volume ratio.

3. Results and discussion

Fig. 2 shows the XRD patterns of as-prepared HfO_2 obtained directly after combustion. XRD analysis shows that phase pure HfO_2 with monoclinic phase [$P2_1/c(14)$] was formed in the combustion process itself. The spectrum was compared with the standard one (JCPDS 43-1017) and all the peaks including the minor ones are indexed accordingly. The particle size calculated from full width half maximum (FWHM) using Scherrer formula for the major (1 0 0) reflection of Fig. 1 is found to be ~15 nm.

In order to confirm the monoclinic phase, Raman spectrum of the as-prepared samples were taken and are shown in Fig. 3. There are 36 phonon modes predicted for m-HfO_2, wherein 18 modes ($9A_g + 9B_g$) are Raman active and 15 modes ($8A_u + 7B_u$) are IR active, the remaining three modes being the acoustic modes. There are three IR active modes and three Raman active modes for t-HfO_2. Only one IR active mode is predicted for c-HfO_2 [21,22]. The Raman spectrum of the HfO_2 samples of the present study show 15 Raman modes, indicating that the HfO_2 samples of the present study crystallizes in monoclinic phase, which corroborates our XRD results, and indicate that the phase formation is complete in the combustion process itself. The Raman peak positions of the samples of the present study are again compared with that of the reported data for bulk HfO_2 [21]. It can be found from the previously reported data that the three Raman active modes of m-HfO_2 are absent and one IR active mode (A_u mode at 398) is present in the Raman spectra

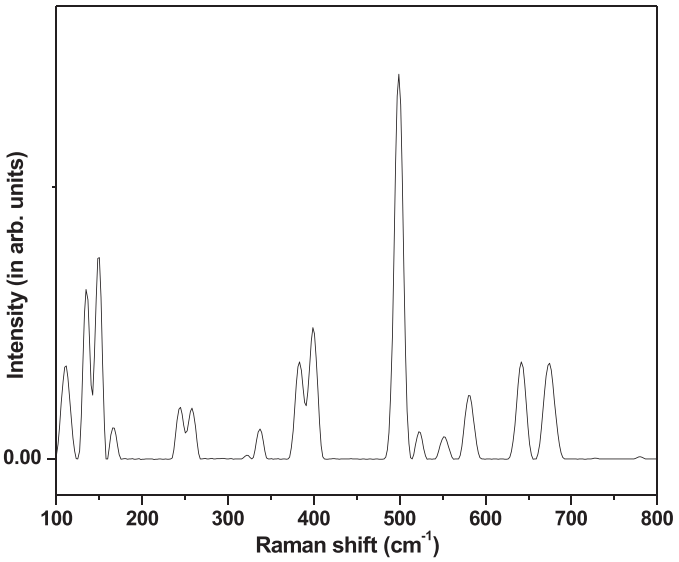

Fig. 3. Raman spectra of as-prepared HfO_2.

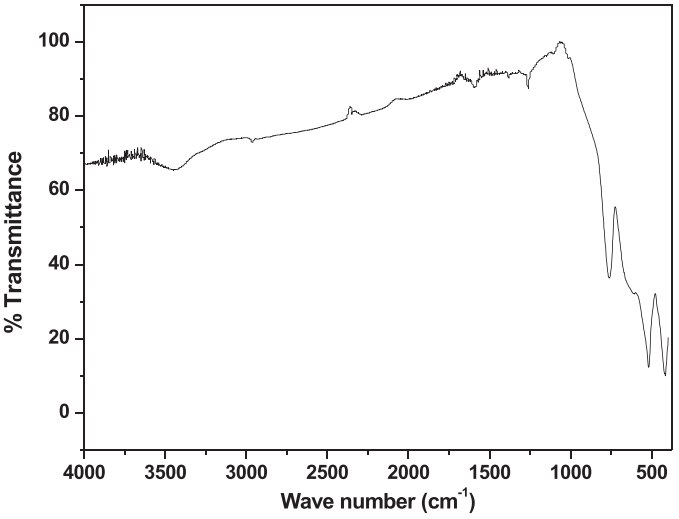

Fig. 4. FT-IR spectra of as-prepared HfO_2.

of samples of the present study. Also, it can be observed that the peak values are shifted to higher frequencies compared to bulk m-HfO_2. The absence of three Raman peaks and the presence of peak at 398 cm^{-1} and the shift in the Raman peaks can be attributed to phonon confinement effect in nanocrystals.

Fig. 4 shows the FT-IR spectra of the as-prepared HfO_2 powders in the range 400–4000 cm^{-1}. From the FT-IR spectra, it is clear that no organic impurities, carbonates or nitrates, etc. are present in the as-prepared sample. Also the FT-IR spectra are found to be matching with that of earlier reports of HfO_2 [1]. Thus X-ray diffraction, Raman and infrared spectroscopic studies confirm that the phase formation is complete in a single-step combustion process itself.

Fig. 5a shows the transmission electron microscopic image of as-prepared HfO_2 and Fig. 5b shows the corresponding selected area electron diffraction pattern. From the TEM image, it is clear that the nanoparticles of HfO_2 having the particle size of the order of about 10–15 nm is obtained in the combustion process. The ring nature of the electron diffraction pattern is indicative of the poly-crystalline nature of the crystallites, but the spotty nature of the SAED pattern in figure can be due to the fact that the finer crystallites having related orientations are agglomerated together

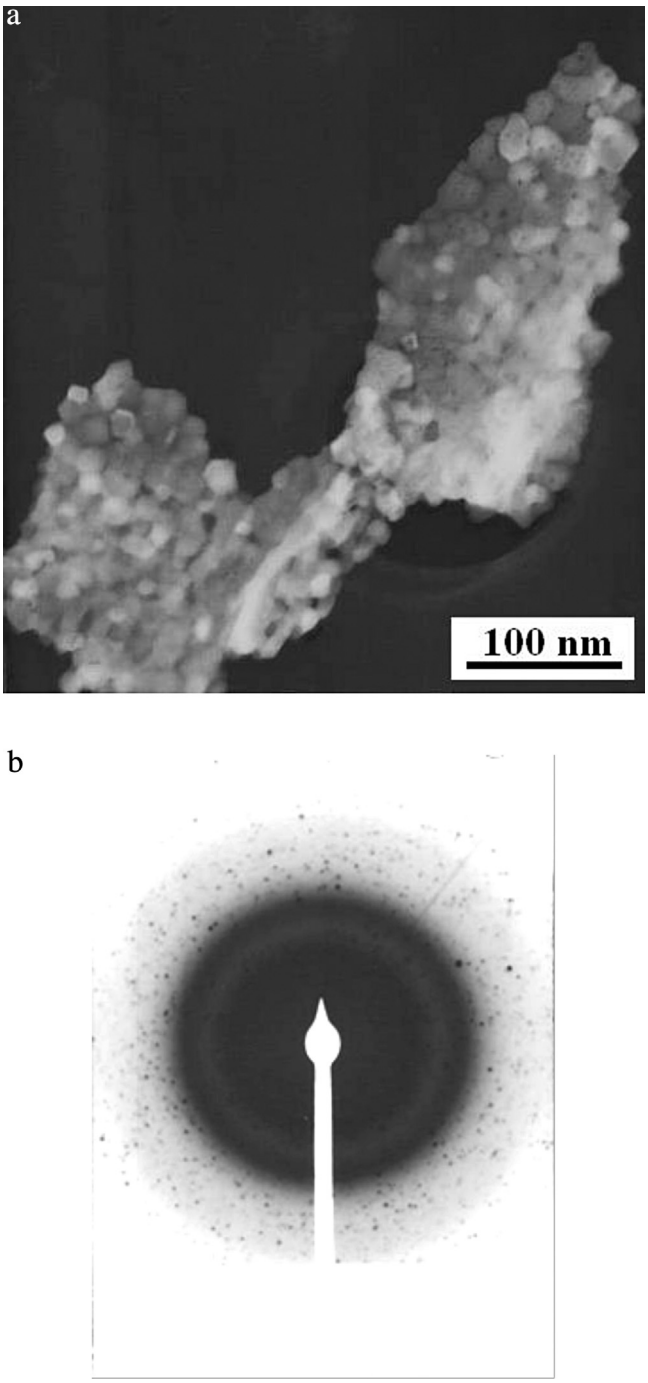

Fig. 5. (a) TEM image of as-prepared HfO_2. (b) SAED pattern of as-prepared HfO_2.

resulting in a limited set of orientations. Due to the ultrafine nature of the nanopowders, which is of the order of 10–15 nm, the ring nature of SAED pattern is limited.

The optical absorbance, transmittance, and reflectance spectra of the HfO_2 nanopowder are shown in Fig. 6. The maximum absorbance occurred within the UV region from where the absorbance decreased with the wavelength towards the NIR region. The transmittance increased exponentially from the UV region towards the NIR region. The transmission spectrum showed that the sample exhibits transmittance of about 85% in the NIR region. The properties of poor transmittance in the UV but moderately high transmittance in the VIS-NIR regions make it an excellent material for screening off UV portion of electromagnetic spectrum in

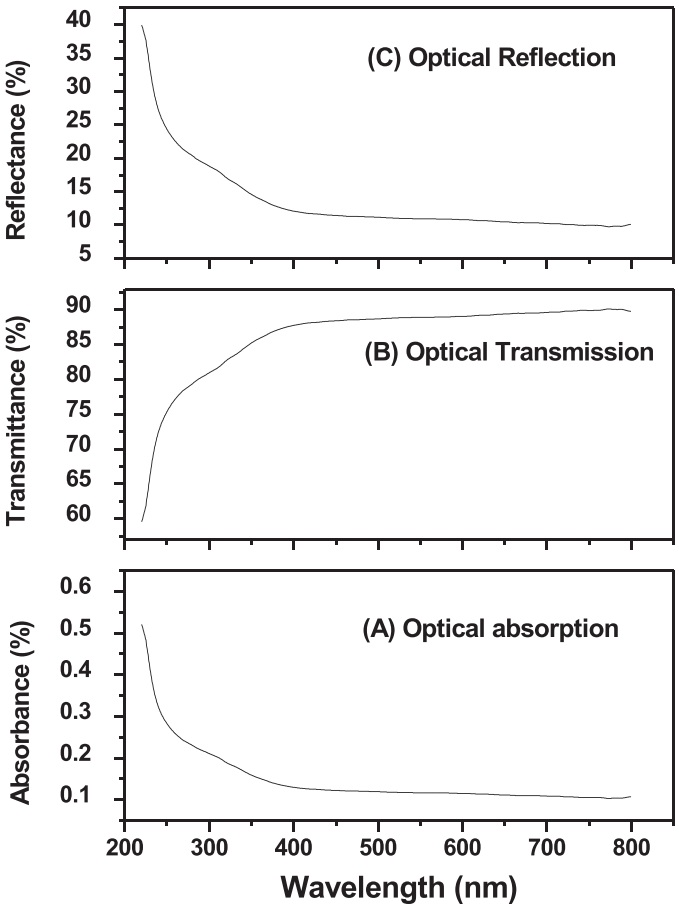

Fig. 6. Optical absorption, transmission and reflection spectra of nanocrystalline HfO_2.

UV filters and sensors. The optical absorption in the shorter wavelength region is mainly attributed to the electron transition from the top of the valence band to the bottom of the conduction band [23]. The property of high transmittance and low reflectance in the visible region makes the material a good candidate as transparent windows in solar cells.

A material can be characterized as a semiconductor or an insulator by determining its band gap energy. According to Wood and Tauc the E_g is associated with absorbance and photon energy by the following equation:

$$(\alpha h\nu) = \beta(h\nu - E_g)^m$$

where α is the absorbance, h is the Planck constant, ν is the frequency, E_g is the optical band gap, and m is a constant associated to the different electronic transitions as $m = ½, 2, 3/2, 3$ for direct allowed, indirect allowed, direct forbidden and indirect forbidden transitions, respectively [24]. The band gap can be obtained from the extrapolation of the straight-line portion of $(\alpha h\nu)^{1/m}$ vs. $h\nu$ plot to $h\nu = 0$.

The optical absorption coefficient α is determined using the relation

$$\alpha = -\ln\frac{\tau}{d}$$

where T is the optical transmittance and d is the optical path length through the cuvette. The variation of α with photon energy is shown in Fig. 7. The absorption edge was found at shorter wavelength in UV region at 248 nm. The existence of sharp absorption edge is the characteristics of crystalline state of the material which corroborates the XRD analysis. It is clear that α has maximum value in the

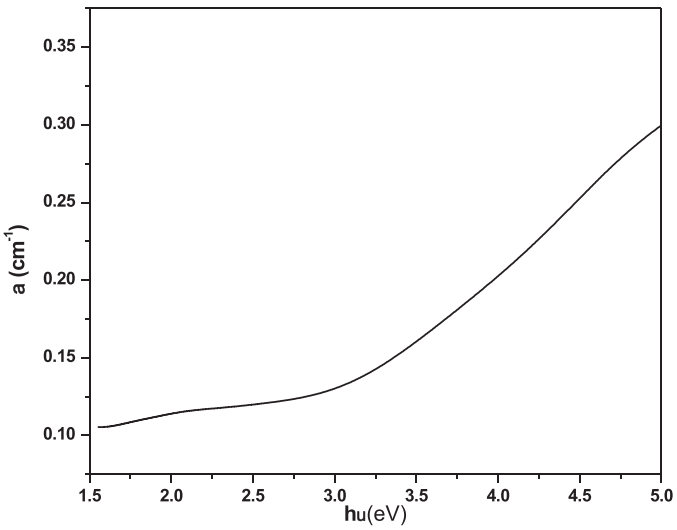

Fig. 7. Variation of absorption coefficient (α) with photon energy for nano-HfO_2.

UV region from where it decreases with wavelength towards NIR region.

The monoclinic HfO_2 structure is reported as an indirect band gap material [25,26]. The band gap energy E_g of HfO_2 nanoparticles was calculated using $m = 2$ and extrapolating the linear portion of the curve or tail as shown in Fig. 8. The obtained result indicated an E_g of 5.1 eV which is lower than those reported in the literature [27,28]. A possible explanation for this phenomenon can be due to oxygen vacancies, distortions on the [HfO_6], intrinsic surface effects, etc. These factors have contributed to the formation of intermediate levels between the valence and conduction band resulting in the decrease of band gap energy. However our result is in good agreement with that reported for a monoclinic HfO_2 [29].

The complex refractive index ($n = n + ik$) and dielectric function ($\varepsilon = \varepsilon_1 + i\varepsilon_2$) characterize the optical properties of any solid material. The normal incidence reflectivity R [30] can be given by

$$R = \frac{(n-1)^2 + k^2}{(n+1)^2 + k^2}$$

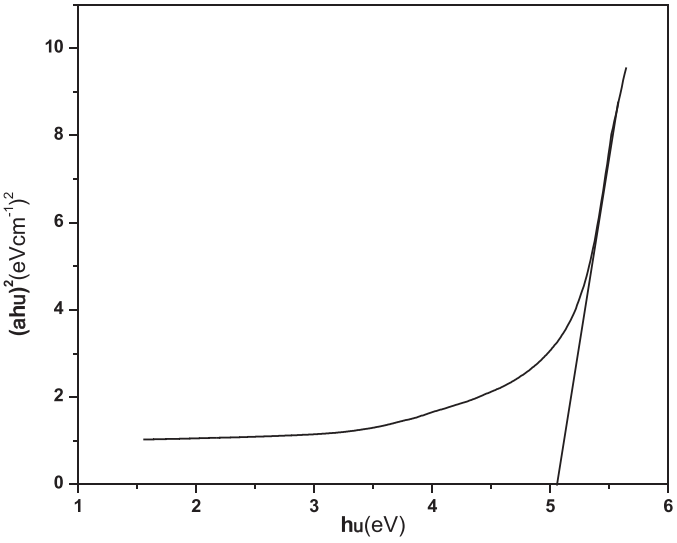

Fig. 8. Tauc's plot for nanocrystalline HfO_2.

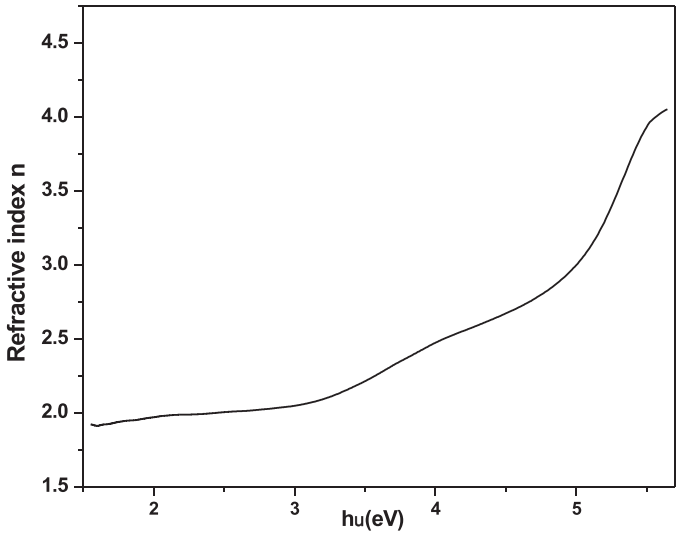

Fig. 9. Variation of refractive index with photon energy for nano-HfO_2.

where k is the extinction coefficient which indicates the amount of absorption loss when the electromagnetic wave propagates through the material [31] and can be calculated using the relation

$$k = \frac{\alpha\lambda}{4\pi}$$

The variations of n and k with photon energy are shown in Figs. 9 and 10 respectively. The refractive index n and extinction coefficient k decreases with increasing wavelength. The refractive index changes with variation of wavelength of the incident light beam due to the interactions between photons and electrons. It is found that n and k show maximum at the same photon energy 5.640 eV. The nanocrystalline HfO_2 prepared was observed to be a semiconductor at room temperature since the maximum value of refractive index (n) occurred at energy ranges near where the maximum change in k occurred [32]. The peak values of n and k observed in the UV region indicate that the material is an inorganic UV absorber.

The fundamental electron excitation spectrum of the nanopowder was described by means of a frequency dependence of the complex electronic dielectric constant. The complex dielectric constant is a fundamental intrinsic material property. The dielectric

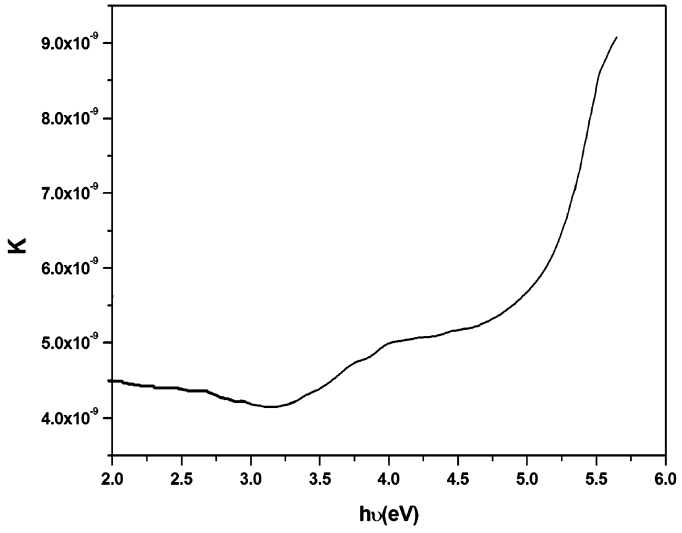

Fig. 10. Variation of extinction coefficient (k) with photon energy for nano-HfO_2.

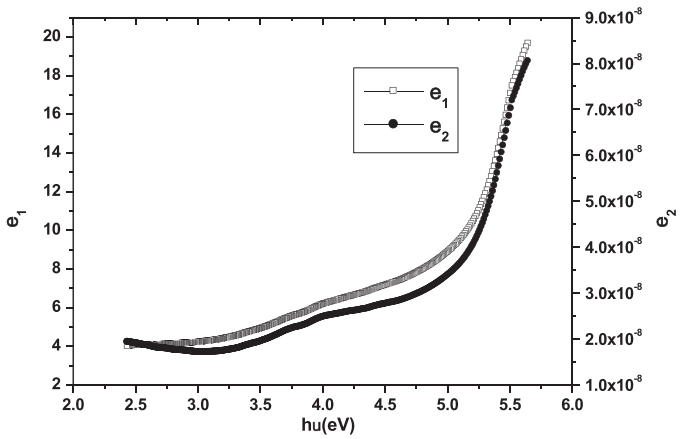

Fig. 11. Variation of real and imaginary dielectric constant with photon energy for nano-HfO_2.

functions ε_1 and ε_2 are related to the complex index of refraction n and k by the following equations: $\varepsilon_1 = n^2 - k^2$ and $\varepsilon_2 = 2nk$ [33].

The variation of real and imaginary dielectric constant with photon energy is plotted and shown in Fig. 11. Both ε_1 and ε_2 increases with photon energy and attains maximum of 20 at 5.5 eV photon energy. The value of real dielectric constant is in good agreement with the earlier reported value [34].

The optical conductivity of the sample is determined using the relation [35]

$$\sigma = \frac{\alpha nc}{4\pi}$$

where c is the velocity of light.

Fig. 12 shows the variation of optical conductivity with incident photon energy. It is seen from the figure that the optical conductivity increases with increasing energy. This suggests that the increase in optical conductivity with frequency is due to the electrons excited by photon energy.

The PL spectra of nano-HfO_2 are shown in Fig. 13. The sample gives a broad emission peak in the red region centred at 628 nm. Usually HfO_2 is reported to give a green emission in the visible region. Here the red emission can be attributed to the oxygen vacancies in the as-prepared samples. Oxygen vacancies are considered as key factors in the PL behaviour of HfO_2. The electron paramagnetic resonance study of HfO_2 reveals the presence of Hf^{3+} defects into the structure acting as charge trapping centres on

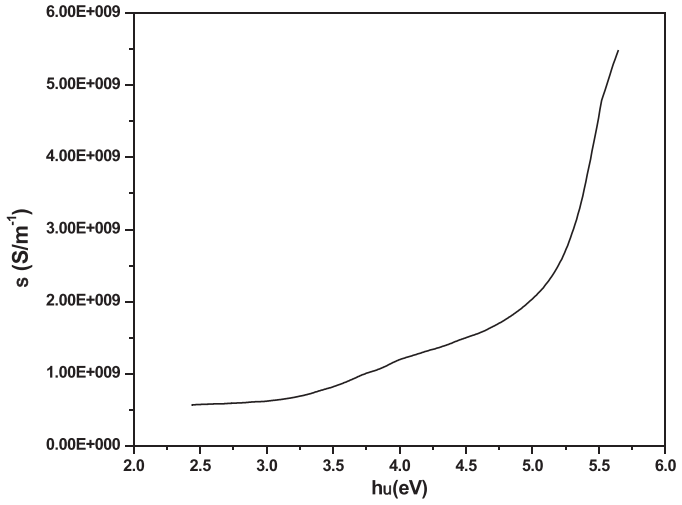

Fig. 12. Variation of optical conductivity with photon energy for nano-HfO_2.

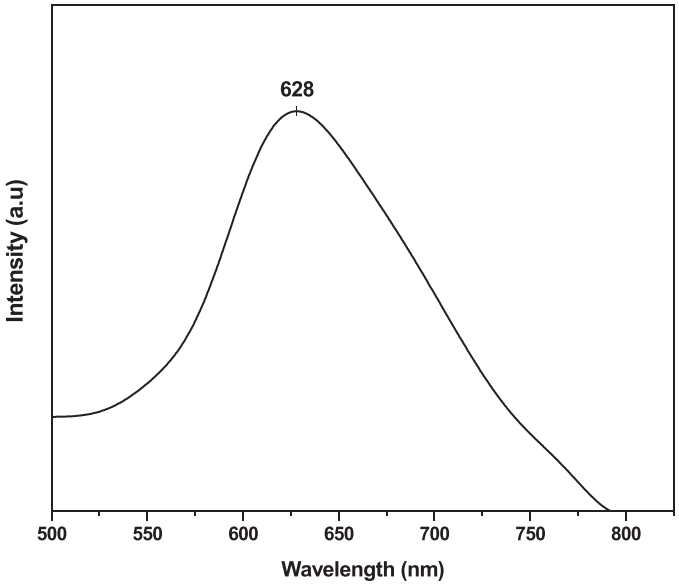

Fig. 13. Photoluminescent spectra of nano-HfO_2.

the surface [36]. The process of combustion lasts only for a few seconds and the powders so obtained are nanostructured in size, and may cause oxygen vacancies in the samples. These oxygen vacancies cause slight distortions in the crystalline structure that have resulted in the formation of intermediate energy levels [37]. It has already been reported that the oxygen vacancies in HfO_2 cause photoluminescent emission around 600–650 nm [38]. The presence of intermediate levels is also identified from the UV–vis spectrum which is stated as the reason for decrease in band gap energy. These results are in good agreement with the earlier reports [36–38].

4. Conclusions

Nanocrystalline HfO_2 was prepared using a single-step auto-igniting combustion technique from $HfCl_4$. X-ray diffraction studies reveal that the HfO_2 crystallizes in the monoclinic phase [$P2_1/c(14)$] and the particle size calculated from FWHM was found to be 15 nm which is in good agreement with the TEM results. FT-IR and FT-Raman spectroscopic studies confirm the monoclinic phase [$P2_1/c(14)$] of the as-prepared HfO_2. All these studies confirm that the phase formation is complete during the combustion synthesis itself without the need of any calcinations steps. The optical properties of the samples as well as the band gap were analysed using UV spectroscopic techniques and the optical constants were determined. The refractive index and the excitation coefficient were calculated from the reflectance spectrum. The transmission spectrum showed that the sample exhibits transmittance of about 85% in the near-infrared region and poor transmittance in the UV region. This indicates that the sample can be used as UV filters and sensors. The band gap of nanocrystalline HfO_2 was found to be 5.1 eV, which was found to be low compared to the values reported for bulk HfO_2. The photoluminescent spectra of nanocrystalline HfO_2 was recorded and spectrum showed a broad emission at 628 nm. The low band gap, as well as broad photoluminescent spectra, indicates the presence of intermediate energy levels in nanocrystalline HfO_2.

Acknowledgement

The author H. Padma Kumar acknowledges the financial aid from Science and Engineering Research Board (SERB), Department of Science and Technology, Ministry of Science and Technology, Government of India, New Delhi, India, under the scheme Fast Track Scheme for Young Scientists (SR/FTP/PS-070/2010).

References

[1] J. Tang, J. Fabbri, R.D. Robinson, Y. Zhu, I.P. Herman, M.L. Steigerwald and L.L.E. Brus, Chem. Mater., 16, 1336–1342 (2004).
[2] G.D. Wilk, R.M. Wallace and J.M. Antony, J. Appl. Phys., 89, 5243–5275 (2001).
[3] C. Giuri, M.R. Perrone and V. Piccinno, Appl. Opt., 36, 1143–1148 (1997).
[4] M.F. Al-Kuhali, Opt. Mater., 27, 383–387 (2004).
[5] I.R. Magunov, R.L. Magunov and G.P. Kornitskiy, Funct. Mater., 8, 563–565 (2001).
[6] S.M. Edlou, A. Smajkiewicz and G.A. Al-Jumaily, Appl. Opt., 32, 5601–5605 (1993).
[7] M. Gilo and N. Croitoru, Thin Solid Films, 350, 203–208 (1999).
[8] F. Cardarelli, Materials Handbook, 2nd ed., Springer, London (2000).
[9] H. Gleiter, Acta Mater., 48, 1–29 (2000).
[10] C. Suryanarayana, Bull. Mater. Sci., 17, 307–346 (1994).
[11] C.H. Lu, H.C. Hong and R. Jagannathan, J. Mater. Chem., 12, 2525–2530 (2002).
[12] V. Kiisk, S. Lange, K. Utt, T. Tatte, H. Mandar and I. Sildos, Physica B, 405, 758–762 (2010).
[13] S. Pavasupree, Y. Suzuki, S. Pivsa-Art and S. Yoshikawa, Ceram. Int., 31, 959–963 (2005).
[14] W.T. Tang, Z.F. Ying, Z.G. Hu, W.W. Li, J. Sun, N. Xu and J.D. Wu, Thin Solid Films, 518, (9) 5442–5446 (2010).
[15] S.J.L. Ribeiro, Y. Messaddeq, R.R. Goncalves, M. Ferrari, M. Montana and M.A. Aegerter, Appl. Phys. Lett., 77, 3502–3504 (2000).
[16] P.E. Meskin, F.Y. Sharikov, V.K. Ivanov, B.R. Chuagulov and Y.D. Tretyakov, Mater. Chem. Phys., 104, 439–443 (2007).
[17] T. Mimami and K.C. Patil, Mater. Phys. Mech., 4, 134–137 (2001).
[18] A.G. Merzhanov, J. Mater. Chem., 14, 1779–1786 (2004).
[19] R.C. Patil, S. Radhakrishnan, S. Pethkar and K. Vijaymohan, J. Mater. Res., 16, 1982–1988 (2001).
[20] J. James, R. Jose, A.M. John, J. Koshy, US Patent No. 6,761,866 (2004).
[21] C.W. Li, M.M. McKerns and B. Fultz, Phys. Rev. B, 80, 54304 (2009).
[22] X. Zhao and D. Vanderbilt, Phys. Rev. B, 25, 233106 (2002).
[23] L.B. Duan, G.H. Rao, Y.C. Wang, J. Yu and T. Wang, J. Appl. Phys., 104, 013909 (2008).
[24] J. Tauc, Amorphous and Liquid Semiconductors, Plenum, New York (1974).
[25] J.W. Park, D.K. Lee, D. Lim, H. Lee and S.H. Choi, J. Appl. Phys., 104, 033521 (2008).
[26] D.M. Ramo, J.L. Gavartin and A.L. Shluger, Phys. Rev. B, 75, 205336 (2007).
[27] M.C. Cheynet, S. Pokrant, F.D. Tichelaar and J.L. Rouvière, J. Appl. Phys., 101, 054101 (2007).
[28] N.V. Nguyen, A.V. Davydov, D.C. Horowitz and M.M. Frank, Appl. Phys. Lett., 87, 192903 (2005).
[29] H.Y. Yu, M.F. Li, B.J. Cho, C.C. Yeo, M.S. Joo, D.L. Kwong, J.S. Pan, C.H. Ang, J.Z. Zheng and S. Ramanathan, Appl. Phys. Lett., 81, 376–378 (2002).
[30] O.S. Heavens, Optical Properties of Thin Solid Films, Dover, New York (1965).
[31] E. Marquez, J. Ramirez, P. Villares, R. Jimenez, P.J.S. Ewen and A.E. Owen, J. Phys. D, 25, 535–541 (1992).
[32] D.L. Greenway and G. Harbeke, Optical Properties and Band Structures of Semiconductors, Pergamon, New York (1969).
[33] E. Marquez, A.M. Bernal-Oliva, J.M. Gonzalez-Leal, R. Prieto-Alcon, A. Ledesma, R.J. Garay and I. Martil, Mater. Chem. Phys., 60, 231–239 (1999).
[34] M.N. Jones, Y.W. Kwon and D.P. Norton, Appl. Phys. A, 8, 285–288 (2005).
[35] F. Tepehan and N. Ozer, Sol. Energy Mater. Sol. Cells, 30, 353–365 (1993).
[36] S. Wright and R.C. Barklie, J. Mater. Sci. Mater. Electron., 18, 743 (2007).
[37] S.A. Eliziario, L.S. Cavalcante, J.C. Sczancoski, P.S. Pizani, J.A. Varela, J.W.M. Espinosa and E. Longo, Nanoscale Res. Lett., 4, 1371–1379 (2008).
[38] J. Ni, Q. Zhou, Z. Li and Z. Zhang, Appl. Phys. Lett., 93, 011905 (2008).